Inorganic Chemistry

Article

pubs.acs.org/IC

New Iron(II) Spin Crossover Coordination Polymers $[Fe(\mu\text{-atrz})_3]X_2\cdot 2H_2O$ (X = ClO_4^-, BF_4^-) and $[Fe(\mu\text{-atrz})(\mu\text{-pyz})(NCS)_2]\cdot 4H_2O$ with an Interesting Solvent Effect

Yu-Chun Chuang,[†] Chi-Tsun Liu,[†] Chou-Fu Sheu,[†] Wei-Lun Ho,[†] Gene-Hsiang Lee,[‡] Chih-Cheh Wang,[§] and Yu Wang*[,†]

[†]Department of Chemistry, National Taiwan University, Taipei, Taiwan

[‡]Instrumentation Center, College of Science, National Taiwan University, Taipei, Taiwan

[§]Department of Chemistry, Soochow University, Taipei, Taiwan

Supporting Information

ABSTRACT: A potential bridging triazole-based ligand, atrz (*trans*-4,4′-azo-1,2,4-triazole), is chosen to serve as building sticks and incorporated with a spin crossover metal center to form a metal organic framework. Coordination polymers of iron(II) with the formula $[Fe(\mu\text{-atrz})_3]X_2\cdot 2H_2O$ (where X = ClO_4^- (**1**·2H_2O) and BF_4^- (**2**·2H_2O)) in a 3D framework and $[Fe(\mu\text{-atrz})(\mu\text{-pyz})(NCS)_2]\cdot 4H_2O$ (**3**·4H_2O) in a 2D layer structure were synthesized and structurally characterized. The magnetic measurements of **1**·2H_2O and **2**·2H_2O reveal spin transitions near room temperature; that of **3** exhibits an abrupt spin transition at ∼200 K with a wide thermal hysteresis, and the spin transition behavior of these polymers are apparently correlated with the water content of the sample. Crystal structures have been determined both at high spin and at low spin states for **1**·2H_2O, **2**·2H_2O, and **3**·4H_2O. Each iron(II) center in **1**·2H_2O and **2**·2H_2O is octahedrally coordinated with six μ-atrz ligands, which in turn links the other Fe center forming a strong three-dimensional (3D) network; counteranion and water molecules are located in the voids of the lattice. The FeN_6 octahedron of **3**·4H_2O is formed with two atrz, two pyrazine (pyz) ligands, and two NCS^- ligands, where the ligands atrz and pyz are bridged between iron centers forming a 2D layer polymer. A zigzag chain of water molecules is found between the layers, and there is a distinct correlation between the thermal hysteresis with the amount of water molecules the exist in the crystal.

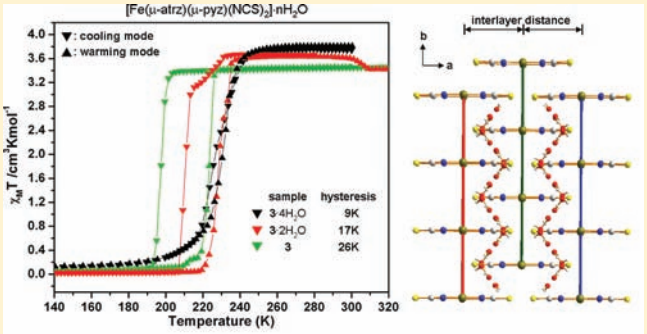

INTRODUCTION

The spin crossover (SCO) system in octahedrally coordinated 3d-metal (with $3d^{4-7}$) complexes has drawn great attention due to its bistable nature of spin states, namely, high spin (HS) and low spin (LS). It is known that the spin transition of a SCO system can be induced under external perturbations such as light irradiation, variation in temperature or in pressure.[1−4] Such unique bistable characters may lead to potential applications in molecular switch, display, memory device, and intelligent contrast agents.[5−8] Incorporation of an iron(II) spin crossover (SCO) center in a framework may enhance the cooperative effect on the variations in physical properties, such as optical, magnetic, and dielectric property, due to the spin transition. In some cases, the existence or absence of solvent molecules[9−11] could affect the spin transition behavior of the metal ion. The spin transition temperature, $T_{1/2}$, is not only affected by local coordination of metal ion but also by counteranions and sometimes even by solvent molecules.[12,13] There are many isolated mononuclear iron(II) SCO systems,[14−19] where strong intermolecular interactions, in some cases, are found between iron centers through $\pi-\pi$ interactions or hydrogen bonding.[20−22] In order to greatly enhance such interaction within the crystal lattice, the design of coordination polymers (CP) in a framework incorporating such spin transition character of the metal ion is thus undertaken. The well-known iron(II) SCO−CP in a 2D framework, $[Fe(btr)_2(NCS)_2]\cdot H_2O$ (btr = 4,4′-bis-1,2,4-triazole) is found to exhibit an abrupt spin transition with 25 K hysteresis;[23,24] whereas in a 3D CP, $[Fe(btr)_3](ClO_4)_2$, it is found to show clear two-step spin transitions with two independent iron sites in the lattice.[25] Recently more attention has been drawn in binuclear complexes[26−38] as well as in frameworks[23−25,39−51] of such SCO systems; there are a few 2D and 3D CPs associated with iron(II) SCO centers using triazole-based[23−25,40,51] and pyridine-based[39,41,44−51] ligands, where the magnetic properties were manifested.

It is known that the spin transition can be fine-tuned not only by the ligand but also by the counterions; in some cases the solvent molecules in the lattice could play some role. In one

Received: December 6, 2011
Published: March 29, 2012

   dx.doi.org/10.1021/ic202626c | Inorg. Chem. 2012, 51, 4663−4671

Table 1. Crystallographic Data of $1{\cdot}2H_2O$, $2{\cdot}2H_2O$, and $3{\cdot}4H_2O$ at 300 K and 150 K

compound	$1{\cdot}2H_2O$		$2{\cdot}2H_2O$		$3{\cdot}4H_2O$	
temperature	300 K	150 K	300 K	150 K	300 K	150 K
formula	$C_{12}H_{16}C_{l2}FeN_{24}O_{10}$		$C_{12}H_{12}B_2FeN_{24}F_8$[a]	$C_{12}H_{16}B_2FeN_{24}F_8O_2$	$C_{10}H_{16}FeN_{12}O_4S_2$	
space group	$P2_1/n$	$P2_1/n$	$P2_1/n$	$P2_1/n$	$C2/m$	$C2/c$
a (Å)	8.1901(3)	8.0267(4)	8.1446(4)	8.0112(2)	13.2751(13)	20.4148(7)
b (Å)	20.1869(7)	19.4307(9)	20.2603(8)	19.4392(8)	7.1940(7)	6.7777(3)
c (Å)	8.9629(3)	8.9609(4)	8.8515(4)	8.9648(3)	12.0161(12)	13.2311(5)
β (deg)	90.846(2)	93.286(4)	90.061(3)	93.382(2)	118.667(3)	95.562(2)
V (Å^3)	1481.70(9)	1395.3(1)	1460.60(11)	1393.67(8)	1006.89(17)	1822.11(12)
Z	2	2	2	2	2	4
μ (mm^{-1})	0.781	0.830	0.62	0.66	1.002	1.107
D_{calc} (g/cm^3)	1.756	1.864	1.641	1.806	1.611	1.780
reflns collected/unique/obs.	12436/2614/1843	12936/2456/1585	17212/3364/1593	14394/3175/1971	4911/1258/1172	8377/2086/1408
T_{max}, T_{min}	0.90, 0.89	0.89, 0.89	0.97, 0.95	0.97, 0.95	0.82, 0.75	0.81, 0.70
GOF on F^2	1.197	1.042	0.988	1.022	1.068	1.097
R_1, wR_2[b] ($I > 2\sigma(I)$)	0.0843, 0.2613	0.0611, 0.1531	0.0527, 0.1208	0.0409, 0.0968	0.0394, 0.1071	0.0526, 0.1483
R_1, wR_2[b] (all data)	0.1145, 0.2798	0.1040, 0.1793	0.1368, 0.1540	0.0813, 0.1140	0.0423, 0.1092	0.0805, 0.1657

[a]The anhydrous sample was obtained by preheating the crystal at 350 K. [b]$R_1 = \Sigma||F_o| - |F_c||/\Sigma|F_o|$; $wR_2(F^2) = [\Sigma w|F_o^2 - F_c^2|^2/\Sigma w(F_o^4)]^{1/2}$.

example in 2D CP of $[Fe(btr)_2(NCS)_2]{\cdot}H_2O$, it has been found to lose its SCO property after dehydration.[23,24] Similarly, a nanoporous metal organic framework, $[Fe_2(azpy)_4(NCS)_4]{\cdot}$(guest) (azpy = *trans*-4,4′-azopyridine), which consists of interpenetrated 2D rhombic grids, exhibits an interesting change in magnetic behavior upon absorption−desorption of guest molecules in the crystal lattice,[41] and such a phenomenon is reversible and highly dependent on the guest molecules. In addition, a 2D layer structure, [Fe(4,4′-bipyridine)$_2$(NCX)$_2$]·*n*Sol (X = S and Se), is recently reported to have a unique SCO property when the solvent content is $4CHCl_3$,[48] and the spin transition is also accompanied with a structural phase transition; however, when the chloroform molecules are removed or replaced by other solvents, e.g., nitrobenzene, nitromethane, toluene, acetone (n = 1−3), etc.,[52] it loses the SCO property. The solvent molecules of such a SCO-CP do play important roles in the spin transition behavior.

We report here three CPs constructed by potentially multidentate ligands, *trans*-4,4′-azo-1,2,4-triazole (atrz).[53,54] Two polymers, $[Fe(\mu\text{-atrz})_3]X_2{\cdot}2H_2O$; X = ClO_4^- ($1{\cdot}2H_2O$) and BF_4^- ($2{\cdot}2H_2O$), in 3D framework exhibit spin transitions near room temperature. The other polymer in the 2D layer structure, $[Fe(\mu\text{-atrz})(\mu\text{-pyz})(NCS)_2]{\cdot}4H_2O$ ($3{\cdot}4H_2O$), also displays a spin transition. The structures and magnetic properties are investigated at various temperatures as well as in the presence and absence of water molecules. Our focus is directed toward a fundamental understanding of the structural and magnetic properties relationship to elucidate the factors, such as different counteranions, guest molecules that affect the spin transition behavior.

EXPERIMENTAL SECTION

All chemicals of reagent grade were purchased and used without further purification.

Synthesis of $[Fe(\mu\text{-atrz})_3](ClO_4)_2{\cdot}2H_2O$ ($1{\cdot}2H_2O$). A solution containing 0.249 g (1.5 mmol) of preprepared (Supporting Information. section A) atrz dissolved in 15 mL of distilled water and warmed to 60 °C was then added to a solution containing 0.128 g (0.5 mmol) of $Fe(ClO_4)_2{\cdot}xH_2O$ and a small amount of ascorbic acid dissolved in 15 mL of distilled water. Red single crystals of the compound $1{\cdot}2H_2O$ were obtained by slow evaporation at room temperature within several days. Anal. Calcd for $C_{12}H_{16}N_{24}Cl_2O_{10}Fe$: C, 18.40; H, 2.06; N, 42.92. Found: C, 18.32; H, 2.04; N, 42.98.

Synthesis of $[Fe(\mu\text{-atrz})_3](BF_4)_2{\cdot}2H_2O$ ($2{\cdot}2H_2O$). The synthetic procedure is similar to that of $1{\cdot}2H_2O$ except replacing the iron salt to $Fe(BF_4)_2{\cdot}6H_2O$. After mixing the solution of iron salt and atrz ligand, the solution was taken into an ultrasonic condition for 15 min. The red crystals of $2{\cdot}2H_2O$ were obtained by slow evaporation for three weeks. Anal. Calcd for $C_{12}H_{16}N_{24}B_2F_8O_2Fe$: C, 18.99; H, 2.12; N, 44.32. Found: C, 18.53; H, 2.42; N, 44.46.

Synthesis of $[Fe(\mu\text{-atrz})(\mu\text{-pyz})(NCS)_2]{\cdot}4H_2O$ ($3{\cdot}4H_2O$). A solution containing 0.082 g (0.5 mmol) of atrz and 0.041 g (0.5 mmol) of pyrazine dissolved in 15 mL of water and warmed to 60 °C, then slowly dripped into a solution containing 0.0997 g (0.5 mmol) of $FeCl_2{\cdot}4H_2O$, 0.074 g (1 mmol) of NH_4NCS and a small amount of ascorbic acid dissolved in 15 mL of distilled water. The yellow solution was obtained after sufficient stirring, and a good quality of dark-red crystals were obtained after a couple of days. Anal. Calcd for $C_{10}H_{16}N_{12}O_4FeS_2$: C, 24.60; H, 3.30; N, 34.42. Found: C, 24.56; H, 3.25; N, 34.49.

Magnetic Measurement. The variable-temperature magnetic susceptibility was measured using the Quantum Design MPMS SQUID magnetometer under an applied magnetic field of 2000 Oe. The polycrystalline samples were packed and sealed in a small section of the straw, and the experiments were taken in dc mode up to 400 K. In situ measurements were made with lowering the temperature first from 280 to 2 K, warmed up to 400 K, and then held for 30 min before taking the other cycle. The data were corrected for temperature independent diamagnetism.

Crystallographic Data. Diffraction data of $1{\cdot}2H_2O$, $2{\cdot}2H_2O$, and $3{\cdot}4H_2O$ were collected[55] on a Nonius KappaCCD diffractometer with Mo radiation (λ = 0.710 73 Å). For each compound, data were measured using an omega scan of 0.5°/frame. The software package DENZO[56] was used to obtain the diffraction intensity, and the absorption correction was applied using SORTAV.[57,58] The structures were determined by direct method and was refined with full-matrix least-squares based on F^2 using SHELXS[59] and SHELXL.[60] Hydrogen atoms were located according to the respective geometries. Details of crystallographic data of $1{\cdot}2H_2O$, $2{\cdot}2H_2O$, and $3{\cdot}4H_2O$ at 300 and 150 K are listed in Table 1. Powder X-ray diffraction of **3** was performed at BL01C in NSRRC, recorded at 150 °C on a Mar3450 image plate at the wavelength of 1.00321 Å, where the 2θ angle calibration is based on the standard powder sample CeO_2. The powder sample is packed in a glass capillary. The crystallographic data are deposited in CCDC-855737-855742 ($1{\cdot}2H_2O$, $2{\cdot}2H_2O$, and $3{\cdot}4H_2O$ at 300 and 150 K), 870070 ($1{\cdot}2H_2O$ at 264 K), and 870753 (**3**). The Cambridge

dx.doi.org/10.1021/ic202626c | Inorg. Chem. 2012, 51, 4663−4671

Crystallographic Data Centre (CCDC) can be accessed via www.ccdc.cam.ac.uk/data_request/cif.

Fe K-Edge and L-Edge X-ray Absorption Spectroscopy. Fe $L_{II,III}$-edge absorption spectra were measured at the high-energy spherical grating monochromator (HSGM) beamline of NSRRC. The spectra are recorded in total electron yield using a microchannel plate (MCP). The photon energy is calibrated using 708.5 eV for the main peak of the Fe L_{III} line of α-Fe_2O_3; the entrance and exit slits are set at 30 μm × 30 μm corresponding to an energy resolution of 0.25 eV at the ~700 eV range. Fe K-edge spectra were measured on a 1.8T/25 pole wiggler beamline in fluorescence mode using a sample holder of 6 μm metal mesh made of In. The resolving power of $\Delta E/E$ is up to 1/7000 (operational energy of 1.5 GeV, 100−200 mA). The Si(111) double crystal is employed as the monochromator. The energy calibration is made on the basis of the E_0 of iron foil at 7112 eV. An APD unit is used for the temperature control; the sample is pressed on an In foil to ensure the good thermal conductivity. The chamber is under ~10^{-9} and 10^{-3} Torr for Fe L- and K-edge absorption, respectively.

RESULTS AND DISCUSSION

Description of the Structures of $[Fe(\mu\text{-atrz})_3]X_2\cdot 2H_2O$ (X = ClO_4^- (1·2H_2O), BF_4^- (2·2H_2O)). Compounds 1·2H_2O and 2·2H_2O are isostructural, which are studied at two temperatures, namely, at 300 K when the Fe^{2+} ion is at the HS state, and at 150 K, when Fe^{2+} ion is at the LS state. The same space group, $P2_1/n$, is retained at all temperatures. Other than the counteranions, the cationic $[Fe(\mu\text{-atrz})_3]^{2+}$ part of both 1·2H_2O and 2·2H_2O is the same, in which the crystallographic asymmetric unit consists of $Fe(\mu\text{-atrz})_{1.5}\cdot H_2O$ with both the iron(II) ion and midpoint of one atrz located at the center of inversion, the other atrz ligand is at the general position. The ligand atrz is very similar to that of btr, however, with longer dimension and more rigid in conformation. The iron(II) is coordinated by six μ-atrz ligands in a nearly regular FeN_6 octahedron (Figure 1a and Table 2); each μ-atrz serves as a bridging ligand connecting two iron(II) centers to form a 3D framework viewing down on the *a*-axis displayed in Figure 1b, which is very similar to that of $[Fe(\mu\text{-btr})_3(ClO_4)_2]$,[25] except an exact 3_1 symmetry is found in the cation of $[Fe(\mu\text{-btr})_3]^{2+}$ with two independent Fe sites. However, only one unique Fe site is found in 1·2H_2O and 2·2H_2O. The basic building unit is a cube, and adjacent cubes are then interlocked to each other as depicted in Figure 1c, thus to establish an interpenetrating 3D network. The anion, ClO_4^- (1·2H_2O) or BF_4^- (2·2H_2O), and the water molecules are located in the voids of the 3D framework as displayed in Figure 1b. The bond lengths of Fe−N at 300 K, 2.170−2.187 Å, for 1·2H_2O and 2·2H_2O correspond to the expected value for Fe^{II} at the HS state; those at 150 K, 1.983−2.000 Å, are typical length for Fe^{II} at the LS state, and relevant distances are listed in Table 2. The typical difference of 0.2 Å in Fe−N distances upon spin transition are found elsewhere.[1,14−17] The volumes of FeN_6 octahedron for 1·2H_2O and 2·2H_2O decreases from 14 to 10 Å^3 under HS to LS conversion (Table 2), which is consistent with previous reports.[61] Weak hydrogen bonds between anions, water molecules, and the C−H of the 1,2,4-triazole rings are found (Table S2 in the Supporting Information). The complete dehydration of 1·2H_2O and 2·2H_2O takes place at 100 °C according to TGA (Figure S2 in the Supporting Information); the powder patterns before and after the dehydration are basically the same (Figure S3 in the Supporting Information), indicating that the structure does not change from the dehydration process, and the powder pattern of anhydrous sample, 1, can be fitted well with the single crystal structure

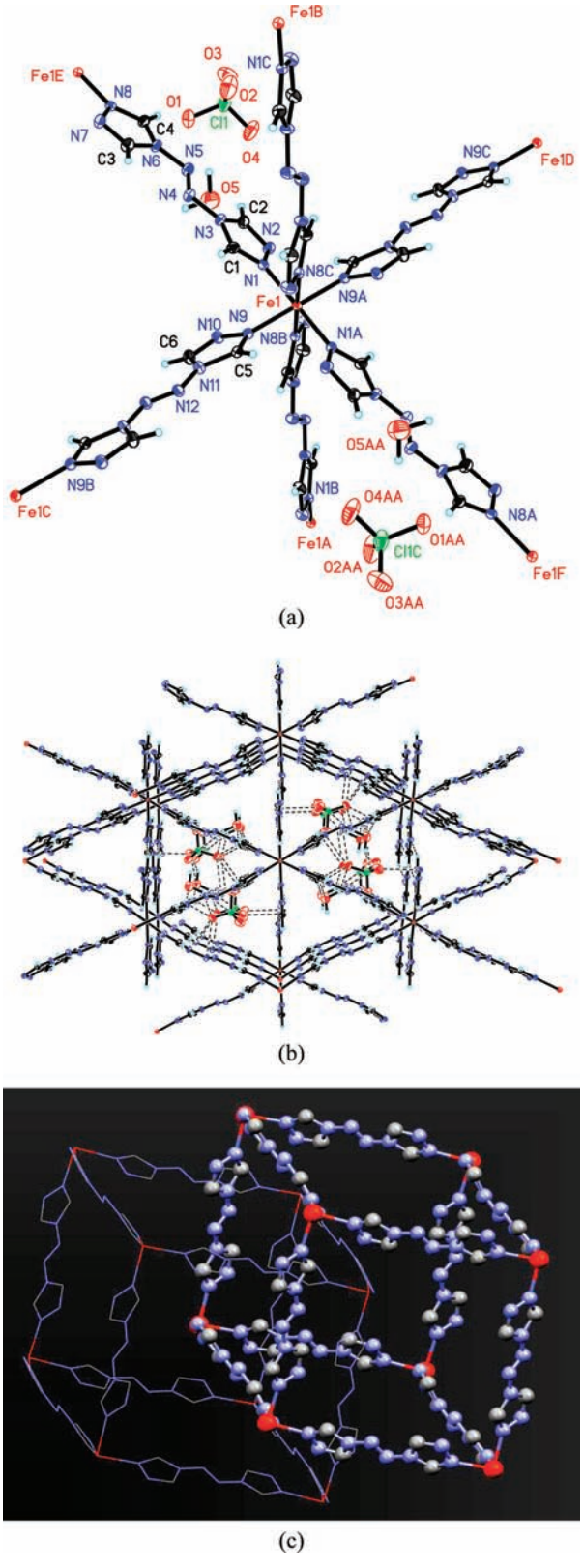

Figure 1. (a) Octahedral coordination geometry around the Fe center of 1·2H_2O with atomic labeling; thermal ellipsoids at 150 K are at 30% probability. (b) Perspective view of the 3D network of $[Fe(\mu\text{-atrz})_3]^{2+}$ viewed along the *a* axis; perchlorate ion and water molecules are located in the voids of the framework (c) Clear view of two interlocked cubes of the building unit.

dx.doi.org/10.1021/ic202626c | *Inorg. Chem.* 2012, 51, 4663−4671

Table 2. Selected Bond Lengths (Å) and Fe···Fe Distances (Å); Volume (Å^3) of FeN_6 Polyhedron for $1{\cdot}2H_2O$, $2{\cdot}2H_2O$, and $3{\cdot}4H_2O$ at 300 K and 150 K

compound	$1{\cdot}2H_2O$		$2{\cdot}2H_2O$		$3{\cdot}4H_2O$		$Fe(btr)_2(NCS)_2{\cdot}H_2O$[23,24]	
temperature	300 K	150 K	300 K	150 K	300 K	150 K	RT	15 K
Fe−N (Å)	2.187(6)	1.987(4)	2.187(3)	1.983(2)	2.204(2)	1.991(3)	2.180(3)	1.9698(5)
	2.173(6)	1.988(4)	2.170(3)	1.984(2)	2.205(2)	1.986(4)	2.188(2)	1.9730(5)
	2.184(6)	2.000(4)	2.183(2)	1.994(2)	2.113(3)	1.951(3)	2.125(3)	1.9498(5)
volume of FeN_6 (Å^3)	13.8	10.5	13.8	10.4	13.7	10.3	13.5	10.1
Fe···Fe through (atrz)	11.801 12.052	11.517 11.682	11.779 12.022	11.521 11.665	12.016	11.614	9.296	8.959
Fe···Fe through (pyz)					7.194	6.678		
Fe···Fe (shortest)	8.19	8.03	8.15	8.01	7.194	6.678	8.46	8.31

without water molecules. The cell parameters and volume thus obtained[62] are nearly the same as well. The temperature dependent cell parameters are monitored in the range of 295 to 200 K, and special attention is paid in the region of 270 to 260 K, where a plateau in $\chi_m T$ is found at 261−269 K. There is no apparent change of cell parameters in the range of 270 to 260 K, and the discontinuity only occurs at the spin transition temperature (Table S4 in the Supporting Information). The crystal structure of $1{\cdot}2H_2O$ at 264 K was tried, but the quality of the crystal was not good due to the twining from the mixed spin states and the number of observed reflections are low. The Fe−N distances thus obtained are between those of typical bond lengths of HS and LS states (Table S3 in the Supporting Information). This is consistent with the hypothesis of a mixture of hydrated and dehydrated forms at this temperature being HS and LS, respectively. The split spots did appear using Cu Kα radiation (Figure S4 in the Supporting Information), nevertheless the differences in cell dimensions are too small to even index the twin cells.

The ligand, atrz, displays a little changes due to the coordination; it is worth noticing that the bond lengths of atrz in $1{\cdot}2H_2O$ where Fe^{II} is at a LS state are very close to those of free ligand. In contrast, more localized features around N(3) in the bonds of triazole ring are found when Fe^{II} is at the HS state, where the N(3)−C(2) and N(3)−C(1) bonds appear to be ∼0.02 Å shorter, and the N(3)−N(4) bond ∼0.03 Å longer than those of the free ligand. The nearly same geometry of the ligand in the complex versus the free ligand may indicate that the coordination is mainly through the nitrogen σ donor. Since the structure of $2{\cdot}2H_2O$ is the same as that of $1{\cdot}2H_2O$, the details of structural description are provided in the Supporting Information, Section F.

Description of the Structure of $[Fe(\mu\text{-atrz})(\mu\text{-pyz})(NCS)_2]{\cdot}4H_2O$ ($3{\cdot}4H_2O$). The layer structure of $3{\cdot}4H_2O$ is built by two different bridge ligands; the rectangular grid is constructed by atrz and pyz ligands at four equatorial sites around each Fe and two NCS anions at axial positions in a trans fashion. The cell parameters at 300 and 150 K listed in Table 1 are in two different space groups. It is monoclinic $C2/m$ at 300 K, where the site symmetry of Fe is C_{2h} (Figure 2a) and becomes $C2/c$ at 150 K with double the cell volume; the site symmetry of Fe is C_2, though the geometry around Fe is the same (Figure 2b) as that of 300 K, with the only difference in the pyz where it is $2/m$ at 300 K but 2 at 150 K. The basic layer structure at two temperatures is essentially the same, which is built by linking the iron centers through the atrz and pyz ligands shown in Figure 2c, where atrz is parallel to the ac plane (according to the cell at 300 K) and the pyz plane is parallel to the ab plane. Water molecules are filled between adjacent layers; there are two independent water molecules in the lattice, and strong hydrogen bonds (O···O distances are 2.594(9) and 2.435(9) Å at 150 K) are found between adjacent water molecules forming a zigzag chain along the b-axis depicted in Figure 2d. One of the water molecules, O(2), is in disorder at 300 K due to the symmetry. Large thermal parameters associated with oxygen atoms are due to the nonstoichiometric content of water molecules. According the TGA measurements, water molecules are removed partially even at room temperature before completely removed beyond 42 °C (Figure S2c in the Supporting Information). The interlayer distance is 5.824 and 5.787 Å, respectively, for the HS and LS state. The Fe−N_{NCS} bond length is 2.113 and 1.951 Å, and ; the bond angle Fe−N−C(S) is close to linear with 172.22° and 177.20° at 300 and 150 K, respectively. The Fe−N_{atrz} bond lengths at HS and LS states are similar to those of $1{\cdot}2H_2O$ and $2{\cdot}2H_2O$, and selected distances are compared in Table 2. The FeN_6 coordination geometry both at HS and at LS states is very close to octahedral geometry, and no significant differences in distortion are found between the HS and LS cases. Unlike the polymer of $[Fe(btr)_2(NCS)_2]{\cdot}H_2O$[23,24] and $[Fe(4,4'\text{-bipyridine})_2(NCS)_2]{\cdot}4CHCl_3$,[48] the bridge ligand, atrz, is perfectly planar both at 300 and 150 K, and the dihedral angle along the azo-bond is zero; whereas in the ligand 4,4′-bipyridine, the angle between the pyridine rings is greater than 38° and that in the btr ligand is ∼90°.

Fe K-Edge and L-Edge X-ray Absorption Spectra of $1{\cdot}2H_2O$. The K-edge absorption at the near edge range (XANES) is known to be sensitive to the coordination symmetry and the oxidation state of the target atom. The Fe K-edge absorption spectra of $1{\cdot}2H_2O$ at 300, 264, and 150 K are shown in Figure 3a. The distinct change in K-edge absorption during the spin conversion is observed and is consistent with the spectra[63] of $[Fe(phen)_2(NCS)_2]$, a well-known SCO complex with abrupt spin transition at 176 K. It is noteworthy that the K-edge at 264 K can be fitted nicely with a mixture of HS and LS. The Fe L-edge absorption spectroscopy is also very sensitive to the electronic changes of Fe atom, especially the changes involving the modification on the 3d orbital population such as the SCO phenomenon. Fe $L_{II,III}$ edges spectra of **1**, the dehydrated form under the high vacuum at 300 and 150 K are displayed in Figure 3b. The absorption peak is shifted to higher energies (1.25 eV for L_{III} and 0.15 eV for L_{II}) at 150 K. The profiles and the relative intensities of HS and LS species are the same as found in $[Fe(phen)_2(NCS)_2]$.[63] The Fe K-edge and L-edge spectra of **2** are the same as those of **1**.

Magnetic Properties. From structure analyses, there are HS (300 K) and LS (150 K) structures for both $1{\cdot}2H_2O$ and $2{\cdot}2H_2O$. The Fe K- and L-edge absorption spectra also depict the respective HS and LS features; however, a mixed HS/LS

dx.doi.org/10.1021/ic202626c | Inorg. Chem. 2012, 51, 4663−4671

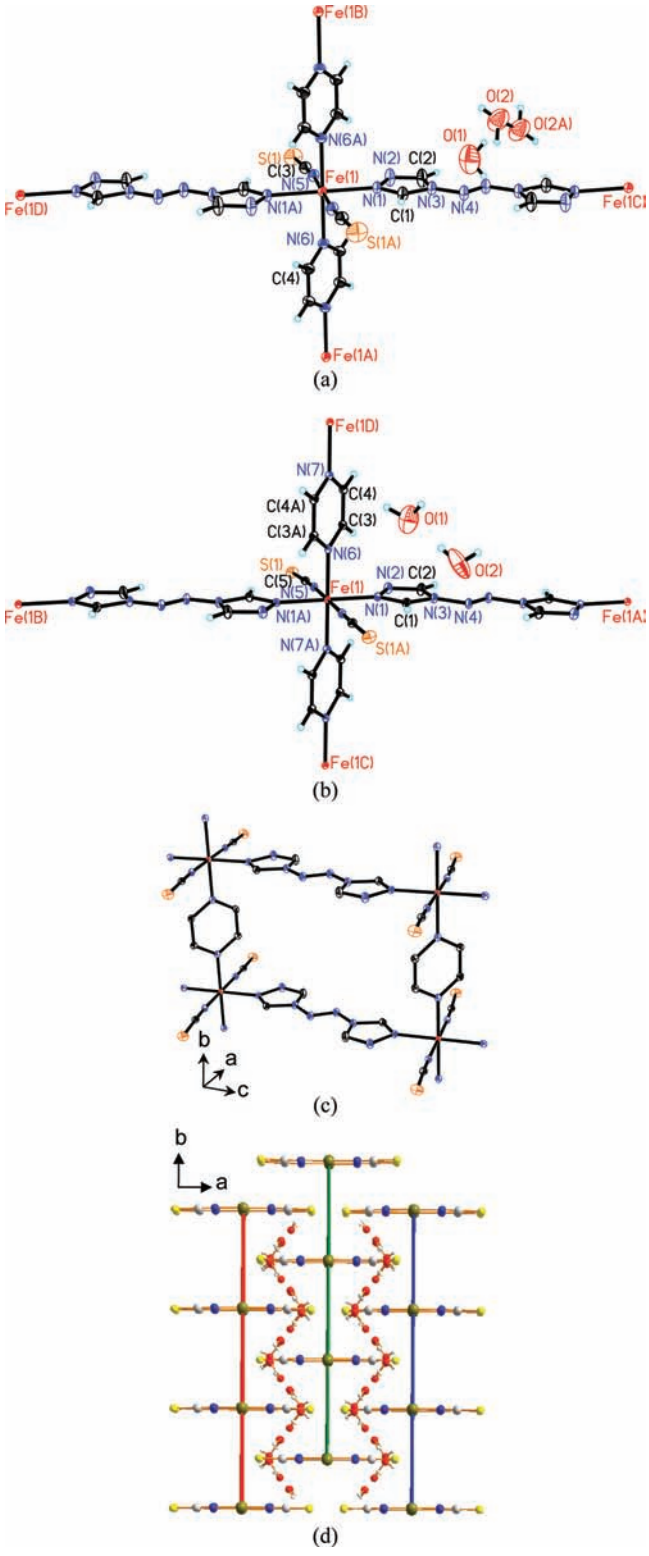

Figure 2. Molecular structure of **3**·4H_2O at (a) 300 K, (b) 150 K, (c) grid unit of the layer structure at 300 K, (d) 1D zigzag chain of water molecules along the *b*-axis between adjacent layers at 300 K, with the layers presented as thick vertical lines for clarity: Fe in green, N in blue, S in yellow, C in gray, and O in red.

configuration exists between 300 and 150 K, hence it might indicate the very gradual spin transition or a stepwise spin transition like that of $[Fe(btr)_3](ClO_4)_2$[25] or an ordering phase transition like that of $[Fe(2\text{-pic})_3]Cl_2$·EtOH (2-pic = 2-

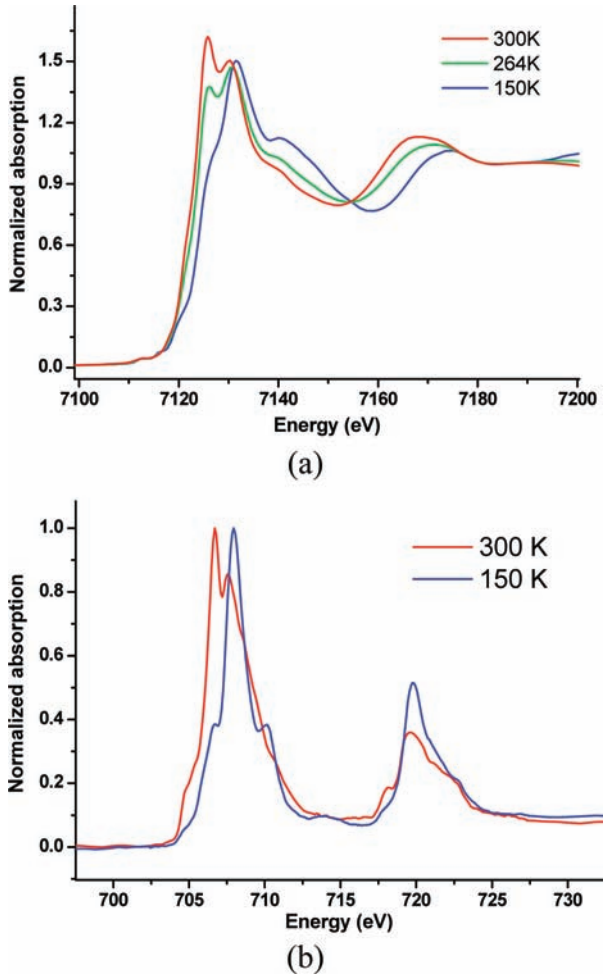

Figure 3. X-ray absorption spectra of **1**·2H_2O (a) Fe K-edge and (b) Fe L-edge. The spectrum in red is measured at 300 K, green at 264 K, and blue at 150 K, respectively.

picolylamine).[64] Yet there is only one unique Fe site in the crystal, and no structural phase change is found in **1**·2H_2O in the range of 300−150 K. The magnetic measurements of **1**·2H_2O and **2**·2H_2O are therefore undertaken. It is displayed in Figure 4 for **1**·2H_2O in the form of the $\chi_m T$ versus T; χ_m being the molar magnetic susceptibility. The $\chi_m T$ is 3.56 cm^3 K mol^{-1} at 300 K, which is in the range of expected values for a HS Fe^{2+} ion. As the temperature is lowered, $\chi_m T$ first remains constant until 290 K and then rapidly decreases to 2.10 cm^3K mol^{-1} at 269 K; again, a plateau appears between 269 and 261 K, below 261 K the $\chi_m T$ falls abruptly to 0.03 cm^3 K mol^{-1} at 200 K; as the temperature increases, it reveals a thermal hysteresis of 2.5 K in the lower step. The plateau ∼264 K is unexpected and is not consistent with the crystal structure where only one unique Fe site exists, yet the Fe K-edge absorption at 264 K also shows a mixture of the HS and LS feature. In order to unravel such uncomprehending magnetic behavior, a more careful in situ measurement is taken: a freshly prepared sample is used, the magnetic susceptibility is measured starting from 280 K and slowly lowering the temperature until 5 K, heating to 400 K gradually (runs 1 and 2), then held at 400 K for 30 min before cooling the sample slowly down to 5 K and warming up back to 300 K (runs 3 and 4). It shows a fairly gradual spin transition down to $\chi_m T$ of 0.3 at 200 K (run 1); when warming up it follows almost the same path with a slight hysteresis of 3 K

dx.doi.org/10.1021/ic202626c | *Inorg. Chem.* 2012, 51, 4663−4671

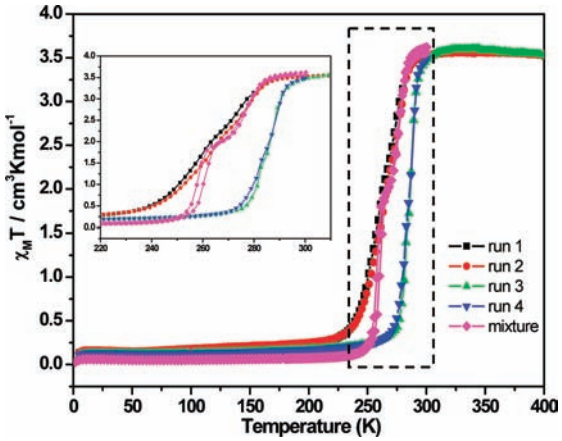

Figure 4. Temperature dependence on $\chi_m T$ for $1{\cdot}2H_2O$. In situ magnetic measurement; run 1 (■) represents the 1st cooling mode; run 2 (red ●) is the warming mode up to 400 K; the 2nd cycle starts after the dehydration, with runs 3 (green ▲), and 4 (blue ▼). Another measurement, pink ♦, is from a different sample which is kept in air for a few days. The inset is the enlargement of the dotted area.

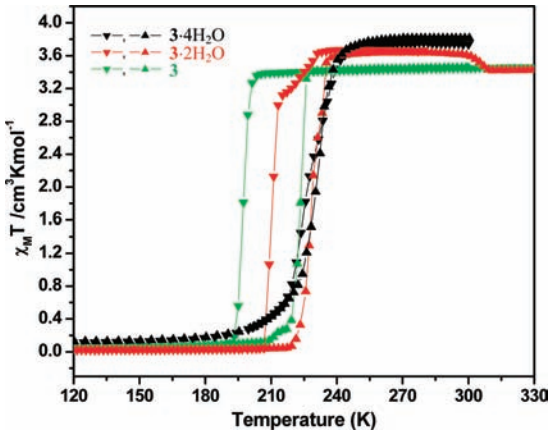

Figure 5. Temperature dependence on $\chi_m T$ for $3{\cdot}nH_2O$ with various water contents: the black, red, and green lines represent n = 4, 2, and 0; ▼ and ▲ represent cooling and warming modes of the cycle, respectively.

around 260 K (run 2). Significant difference in the $\chi_m T$ curve is found in runs 3 and 4, where an abrupt spin transition at 285 K and no thermal hysteresis is found. The subsequent cycles of measurements give the exact same feature as runs 3 and 4. With the help on the TGA (Figure S2 in the Supporting Information), a gradual weight loss of water molecules beyond room temperature is found; complete dehydration takes place above 370 K. Therefore starting from a freshly prepared sample (runs 1 and 2) becomes crucial; the in situ magnetic measurement (runs 3 and 4) after the sample is dehydrated at 400 K yields a higher spin transition temperature (285 K) and a more abrupt one than that of the hydrated one (~265 K). The plateau at 261–269 K can be explained as a mixture of $1{\cdot}2H_2O$ and **1**, since the water molecule is removed at room temperature and the plateau could occur between these two transition temperatures. Such solvent affected magnetic behavior is noticed elsewhere.[9−11,65,66] Similar phenomenon is observed in $2{\cdot}2H_2O$ (Figure S6 in the Supporting Information), but the difference between the hydrated and dehydrated species is not so pronounced.

Keep in mind of the finding in $1{\cdot}2H_2O$, the sample preparations for magnetic measurement are taken carefully: a freshly prepared sample of $3{\cdot}4H_2O$, dry in air (sample a), presumably with four water molecules in the lattice, undergoes a very gradual transition with a hysteresis loop of 9 K ($T_c^{\downarrow}$ = 223 K and $T_c^{\uparrow}$ = 232 K), a maximum $\chi_m T$ value of 3.8 cm^3 K mol^{-1} at 280 K depicted in Figure 5. Another sample was prepared and quickly dried by aspirator (sample b), presumably with close to two water molecules ($3{\cdot}2H_2O$) in the lattice; when sample b is cooled from 280 K with an initial $\chi_m T$ value of 3.6 cm^3 K mol^{-1}, a drop in $\chi_m T$ to 3.0 cm^3 K mol^{-1} was found at 230–210 K, and then an abrupt drop to 0.04 cm^3 K mol^{-1} takes place. As the sample is warmed, the $\chi_m T$ value undergoes a sudden rise to 3.6 cm^3 K mol^{-1} at ~227 K and then a small drop to 3.42 cm^3 K mol^{-1} at 310 K; this drop of 0.18 cm^3 K mol^{-1} corresponds to the weight loss due to the removal of ~2.4 water molecules. The sample is then kept at 400 K for 30 min to ensure the complete removal of water molecules. The subsequent measurements exhibit a very abrupt spin transition with a wider hysteresis of 26 K (197–223 K); the magnetic behavior remains the same in the subsequent runs of the cooling–warming cycle; this certainly corresponds to the anhydrous sample, and similar magnetic measurements can be obtained by preheating the sample at 100 °C. Accordingly, we propose that the different spin transition behaviors arising from three species, i.e., the coordination polymer $3{\cdot}nH_2O$ containing roughly four, two, and zero (n = 4, 2, and 0 based on stoichiometry in the unit cell) water molecules in the lattice, and their spin transition temperatures as well as their thermal hysteresis are listed in Table 3. The drop at 230–210 K in sample b can be interpreted as the presence of the mixture of species of four and two water molecules, ~18% of four water molecule species according to the fit in magnetic susceptibility (Figure S7 in the Supporting Information), which agrees with 2.4 H_2O estimated from the drop at 310 K.

Table 3. Correlations of Spin Transition and Water Contents for $1{\cdot}nH_2O$, $2{\cdot}nH_2O$, and $3{\cdot}nH_2O$

compound	$T_{1/2}^{\downarrow}$ (K)	$T_{1/2}^{\uparrow}$ (K)	hysteresis (K)
$3{\cdot}4H_2O$	223	232	9
$3{\cdot}2H_2O$	210	227	17
3	197	223	26
$Fe(btr)_2(NCS)_2{\cdot}H_2O$[23,24]	120	145	25
	$T_{1/2}$ (hydrated) n = 2	$T_{1/2}$ (dehydrated) n = 0	temperature shift (K)
$1{\cdot}nH_2O$	265	285	20
$2{\cdot}nH_2O$	284	290	6

Relationship between Structure and Magnetic Property. A nearly perfect FeN_6 octahedral geometry of $1{\cdot}2H_2O$ and $2{\cdot}2H_2O$ is formed by the six atrz ligands, which leads to small values in distortion parameters both at the HS and LS state. The Fe···Fe separation through the atrz ligand is ~12 Å at 300 K. However, it is well established that cooperativity is attributed to the efficient communication between SCO centers, which means the connectivity of the coordination network is important. The shortest Fe···Fe separation through the interlocked network is 8.19 Å for $1{\cdot}2H_2O$, which is comparable with those of $[Fe(btr)_3](ClO_4)_2$[25] (8.67 Å at 260 K) and $[Fe(btzb)_3](PF_6)_2{\cdot}$solv (btzb = 1,4-bis(tetrazol-1-yl)butane)[40] (8.84 Å). Within the 3D interpenetrating framework, weak hydrogen bonds exist between water molecules, atrz and counteranions; the water molecule only

dx.doi.org/10.1021/ic202626c | Inorg. Chem. 2012, 51, 4663–4671

weakly interacts with the $[Fe(\mu\text{-atrz})_3]^{2+}$ cation. The spin transition of $\mathbf{1}\cdot 2H_2O$ is much more gradual than that of $\mathbf{2}\cdot 2H_2O$, and the spin transition of both **1** and **2** becomes abrupt and the transition temperature shifts toward higher temperature, approximately 20 K in **1** but only 6 K in **2** after the removal of water molecules. However, the transition temperatures of dehydrated samples of **1** and **2** are almost the same, although counteranions were often found to play some role in the spin transition behavior,[11,67−70] and little difference is found between **1** and **2**; it could be understood that the rigid 3D network structure is totally constructed by the $[Fe(\mu\text{-atrz})_3]^{2+}$ cation, and the counteranions are only located in the voids of the network, and besides the shape and volume of these two anions BF_4^-, (53.4 Å^3) and ClO_4^- (54.4 Å^3) are similar. The spin transition temperature, 285 K, of these two dehydrated compound is close to room temperature and the spin transition is abrupt, which are desired properties for potential applications of magnetic material.[5,71,72] The small plateau at 261−269 K in the $\chi_m T$ curve observed in Figure 4 can be realized as a mixture of hydrated ($\mathbf{1}\cdot 2H_2O$) and dehydrated (**1**) species being at the HS and LS states, respectively, which is evidenced by the Fe K-edge absorption and also by the structure analysis taken at 264 K (Table S3 in the Supporting Information). A similar stepwise spin transition is also observed in the case of $[Fe(btzb)_3](PF_6)_2\cdot$solv,[40] where only one unique iron site exists in a similar 3D framework; this intermediate phase is assumed to be thermodynamic stabilization of alternating HS and LS iron sites, which roughly agrees with the idea on the ordering intermediate phase of $[Fe(2\text{-pic})_3]Cl_2\cdot EtOH$[64] when it becomes in long-range ordering. Of course, we could give rise to the same explanation in $\mathbf{1}\cdot 2H_2O$; however, such dynamic stabilization is associated with the water molecules, since there is no such intermediate phase observed in the dehydrated form **1**.

The 2D layer structure of $\mathbf{3}\cdot nH_2O$ is more flexible than the compact 3D network, and the interlayer distance becomes a factor to modulate the Fe···Fe distance between the adjacent layers. It is known that changes in the nature of the spin transition do occur with changes in the solvent in such 2D layer structures; for example, in the similar structure of $[Fe(btr)_2(NCS)_2]\cdot H_2O$,[23,24] the interlayer distance is 5.56 and 5.58 Å for the HS and LS cases, respectively, and the spin transition is very abrupt with 25 K hysteresis. However, such a distance becomes very short in the dehydrated form,[73] and it loses its SCO property. Recently, a similar layer structure of $[Fe(4,4'\text{-bipyridine})_2(NCSe)_2]\cdot 4CHCl_3$[48] is reported to have an interlayer distance of 7.89 and 7.71 Å for the HS and LS states, respectively, and the spin transition is again abrupt with 6.6 K hysteresis; it also looses SCO property after complete removal of the chloroform molecules or after exchanging to other solvents.[48,52]

The interlayer distance of $\mathbf{3}\cdot 4H_2O$ is 5.82 and 5.79 Å for the HS and LS states, respectively; a one-dimensional zigzag chain of water molecules along the *b*-axis exists between adjacent layers (Figure 2d), and strong hydrogen bonds are found only between the water molecules. The layer structure retains when removal of the water molecules by heating, and only the interlayer distance decreases as the temperature increases; according to the in situ powder X-ray diffraction (Figure S8 in the Supporting Information), the cell parameter "*a*" is reduced as water molecules are removed. A decrease in interlayer distances from 5.82 Å at 300 K to 5.68 Å at 360 K is found (Table S5 in the Supporting Information). In order to confirm that the structure of the dehydrated species (**3**) is the same as that in $\mathbf{3}\cdot 4H_2O$, a structural analysis based on the powder diffraction is undertaken. The agreement between the model and the observed pattern is quite reasonable as shown in Figure 6; the layer structure is essentially unchanged. It is clearly

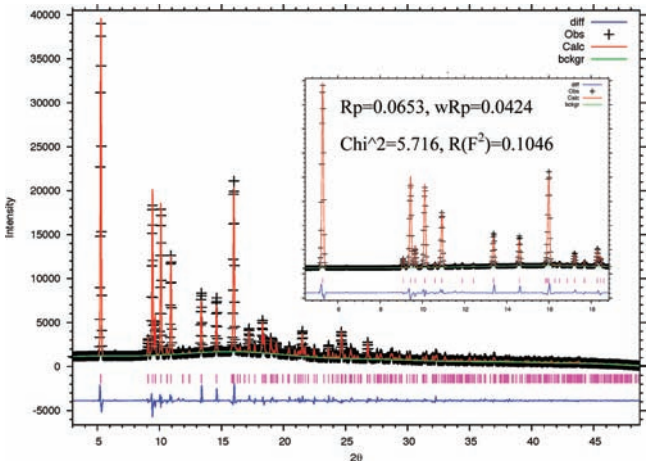

Figure 6. Observed (+) and calculated (red solid line) profiles for the Rietveld refinement of **3**. The bottom curve is the difference intensity; red bars are the Bragg reflections. Crystal data: *C*2/*m*, *a* = 12.6181(4), *b* = 7.1726(2), *c* = 12.0508(4), β = 116.396(2), and volume = 976.94(4).

demonstrated that the amount of water molecules in $\mathbf{3}\cdot nH_2O$ has direct effects on the magnetic behavior of such a polymer; the less water molecules there are, the sharper the spin transition and the wider hysteresis there are (Table 3). In other words, the cooperativity is regulated, in this case, by the chain of water molecules, which may affect the interlayer distance. In this 2D layer structure, the isothiocyanate ligands (SCN−Fe−NCS) are roughly perpendicular to the rectangular grid formed by Fe, pyz, and atrz. There are a few short contacts, such as sulfur to the center of triazole-ring (S···π) and N(2)···H−C_{pyz} interactions (Table S6 in the Supporting Information) between the adjacent layers, which propagate through the lattice and establish a pseudo 3D network structure. Such weak interactions are slightly strengthened by shortening the interlayer distance. Compound $\mathbf{3}\cdot nH_2O$ provides an excellent example to show a systematic correlation on the magnetic behavior with the amount of water molecules in the SCO system. In contrast, those pyridine-based $[Fe(L)_2(NCS)_2]\cdot x$(guest) interpenetrated layer structures[46,47] do not show any apparent thermal hysteresis.

Some mononuclear iron(II) SCO complexes also exhibit a strong solvent effect in magnetic property. $[Fe(2\text{-pic})_3]Cl_2\cdot nH_2O$, is at the LS state when n = 2 where strong hydrogen bonds between chloride ion, 2-pic, and water molecule are found; however, it exhibits an abrupt spin transition with a wide hysteresis of 91 K when n = 1.[74,75] In the case of $[Fe(bpp)_2](BF_4)_2\cdot nH_2O$ (bpp = 2,6-bis(pyrazol−3-yl)pyridine),[12] the anhydrous sample exhibits more abrupt spin transition and lower spin transition temperature with a wider hysteresis loop than the hydrated one, similar to what is found in the 2D layer structure made of $[Fe(pmd)(H_2O)\{Ag(CN)_2\}_2]\cdot H_2O$ (pmd = pyrimidine)[10] and what we observed in **3**. Nonetheless, in all those cases[10,12,74,75] other than $\mathbf{3}\cdot 4H_2O$, a structural phase change is accompanied with the dehydration; unfortunately, no structural information for the

dx.doi.org/10.1021/ic202626c | *Inorg. Chem.* 2012, 51, 4663−4671

dehydrated form is available to establish the structure magnetic relationship. Different magnetic properties of the original and rehydrated samples are disclosed in $[Fe(bpp)_2][Cr(bpy)(ox)_2]\cdot 2H_2O$,[66] which is associated with different structures. In the other polymeric case, even the heating rate (for dehydration) affects the spin transition temperature.[65] In some 1D chainlike Fe^{II}-1,2,4-triazole system and its derivatives,[51] the wide thermal hysteresis loops[5,76] are attributed to the intra- and interchain cooperativity. In the hydrated and dehydrated 2D layer system ($\mathbf{3}\cdot n H_2O$), there are similar intramolecular interactions but slightly different intermolecular interactions. The existence of the chain of water molecules between the layers perhaps weakens the intermolecular interaction and thus weakens the communication between iron centers. Further studies on the guest-dependent magnetic property and structure determination will be helpful.

CONCLUSION

In the present work, 2D/3D frameworks of SCO systems with a strong cooperative effect are presented. Three new spin crossover coordination polymers are synthesized using triazole-based, atrz, and pyrazine ligands. A three-dimensional interlocked metal organic framework is constructed based on two interlocked cube units. It shows an abrupt spin transition at 285 K when the water molecules are removed. The spin transition becomes gradual and toward lower temperature for the hydrated form; however, the structures of the hydrated and dehydrated species are the same. The interesting step in the magnetic susceptibility is understood as a mixture of hydrated and dehydrated forms. The abrupt spin transition of dehydrated species implies that the communication between the iron centers is through the M−L−M framework but would be slightly jeopardized by the presence of water molecules. It is even clearly demonstrated in the layer structure of $\mathbf{3}\cdot n H_2O$, where the width of thermal hysteresis can be regulated with the amount of water molecules between the adjacent layers, again the basic layer structure does not change due to the dehydration.

ASSOCIATED CONTENT

Supporting Information

(A) Synthesis and structure of *trans*-4,4′-azo-1,2,4-triazole (atrz); (B) hydrogen bonds of $\mathbf{1}\cdot 2H_2O$, $\mathbf{2}\cdot 2H_2O$, and $\mathbf{3}\cdot 4H_2O$; (C) TGA measurements of $\mathbf{1}\cdot 2H_2O$, $\mathbf{2}\cdot 2H_2O$, and $\mathbf{3}\cdot 4H_2O$; (D) experimental and simulation powder X-ray diffraction pattern of $\mathbf{1}\cdot 2H_2O$ and **1**; (E) crystallographic result and precession pattern of $\mathbf{1}\cdot 2H_2O$ at 264 K and temperature dependent cell parameters of $\mathbf{1}\cdot 2H_2O$; (F) molecular structure, packing diagram, and magnetic property of $\mathbf{2}\cdot 2H_2O$; (G) simulation of molar magnetic susceptibility of sample b of $\mathbf{3}\cdot 4H_2O$; (H) in situ temperature dependent powder X-ray diffraction experiment of $\mathbf{3}\cdot n H_2O$; and (I) differential scanning calorimetry (DSC) measurements of $\mathbf{1}\cdot 2H_2O$ and **1**. This material is available free of charge via the Internet at http://pubs.acs.org.

AUTHOR INFORMATION

Corresponding Author

*E-mail: wangyu@ntu.edu.tw.

Notes

The authors declare no competing financial interest.

ACKNOWLEDGMENTS

This work is supported by the National Science Council (NSC) and the National Synchrotron Radiation Research Center (NSRRC).

REFERENCES

(1) Gütlich, P.; Garcia, Y.; Goodwin, H. A. *Chem. Soc. Rev.* **2000**, *29*, 419−427.
(2) Gütlich, P.; Hauser, A.; Spiering, H. *Angew. Chem., Int. Ed.* **1994**, *33*, 2024−2054.
(3) Gaspar, A. B.; Muñoz, M. C.; Moliner, N.; Ksenofontov, V.; Levchenko, G.; Gütlich, P.; Real, J. A. *Monatsh. Chem.* **2003**, *134*, 285−294.
(4) Gaspar, A. B.; Ksenofontov, V.; Martinez, V.; Muñoz, M. C.; Real, J. A.; Gütlich, P. *Eur. J. Inorg. Chem.* **2004**, 4770−4773.
(5) Kahn, O.; Martinez, C. J. *Science* **1998**, *279*, 44−48.
(6) Kahn, O.; Kröber, J.; Jay, C. *Adv. Mater.* **1992**, *4*, 718−728.
(7) Muller, R. N.; Vander Elst, L.; Laurent, S. *J. Am. Chem. Soc.* **2003**, *125*, 8405−8407.
(8) Bousseksou, A.; Molnár, G.; Demont, P.; Menegotto, J. *J. Mater. Chem.* **2003**, *13*, 2069−2071.
(9) Hostettler, M.; Törnroos, K. W.; Chernyshov, D.; Vangdal, B.; Bürgi, H.-B. *Angew. Chem., Int. Ed.* **2004**, *43*, 4589−4594.
(10) Niel, V.; Thompson, A. L.; Muñoz, M. C.; Galet, A.; Goeta, A. E.; Real, J. A. *Angew. Chem., Int. Ed.* **2003**, *42*, 3760−3763.
(11) Sato, T.; Nishi, K.; Iijima, S.; Kojima, M.; Matsumoto, N. *Inorg. Chem.* **2009**, *48*, 7211−7229.
(12) Sugiyarto, K. H.; Goodwin, H. A. *Aust. J. Chem.* **1988**, *41*, 1645−1663.
(13) Wei, R. J.; Tao, J.; Huang, R. B.; Zheng, L. S. *Inorg. Chem.* **2011**, *50*, 8553−8564.
(14) Gallois, B.; Real, J. A.; Hauw, C.; Zarembowitch, J. *Inorg. Chem.* **1990**, *29*, 1152−1158.
(15) Niel, V.; Gaspar, A. B.; Muñoz, M. C.; Abarca, B.; Ballesteros, R.; Real, J. A. *Inorg. Chem.* **2003**, *42*, 4782−4788.
(16) Sheu, C. F.; Pillet, S.; Lin, Y. C.; Chen, S. M.; Hsu, I. J.; Lecomte, C.; Wang, Y. *Inorg. Chem.* **2008**, *47*, 10866−10874.
(17) Sheu, C. F.; Chen, S. M.; Wang, S. C.; Lee, G. H.; Liu, Y. H.; Wang, Y. *Chem. Commun.* **2009**, 7512−7514.
(18) Sheu, C. F.; Chen, K.; Chen, S. M.; Wen, Y. S.; Lee, G. H.; Chen, J. M.; Lee, J. F.; Cheng, B. M.; Sheu, H. S.; Yasuda, N.; Ozawa, Y.; Toriumi, K.; Wang, Y. *Chem.—Eur. J.* **2009**, *15*, 2384−2393.
(19) Moliner, N.; Muñoz, M. C.; van Koningsbruggen, P. J.; Real, J. A. *Inorg. Chim. Acta* **1998**, *274*, 1−6.
(20) Weber, B.; Bauer, W.; Obel, J. *Angew. Chem., Int. Ed.* **2008**, *47*, 10098−10101.
(21) Matouzenko, G. S.; Jeanneau, E.; Yu. Verat, A.; Bousseksou, A. *Dalton Trans.* **2011**, *40*, 9608−9618.
(22) Weber, B.; Bauer, W.; Pfaffeneder, T.; Dîrtu, M. M.; Naik, A. D.; Rotaru, A.; Garcia, Y. *Eur. J. Inorg. Chem.* **2011**, 3193−3206.
(23) Vreugdenhil, W.; Van Diemen, J.; De Graaff, R.; Haasnoot, J.; Reedijk, J.; Van Der Kraan, A.; Kahn, O.; Zarembowitch, J. *Polyhedron* **1990**, *9*, 2971−2979.
(24) Legrand, V.; Pillet, S.; Carbonera, C.; Souhassou, M.; Létard, J.-F.; Guionneau, P.; Lecomte, C. *Eur. J. Inorg. Chem.* **2007**, 5693−5706.
(25) Garcia, Y.; Kahn, O.; Rabardel, L.; Chansou, B.; Salmon, L.; Tuchagues, J. *Inorg. Chem.* **1999**, *38*, 4663−4670.
(26) Pelleteret, D.; Clérac, R.; Mathonière, C.; Harté, E.; Schmitt, W.; Kruger, P. E. *Chem. Commun.* **2009**, 221−223.
(27) Nakano, K.; Suemura, N.; Yoneda, K.; Kawata, S.; Kaizaki, S. *Dalton Trans.* **2005**, 740−743.
(28) Garcia, Y.; Robert, F.; Naik, A. D.; Zhou, G.; Tinant, B.; Robeyns, K.; Michotte, S.; Piraux, L. *J. Am. Chem. Soc.* **2011**, *133*, 15850−15853.
(29) Archer, R. J.; Hawes, C. S.; Jameson, G. N. L.; McKee, V.; Moubaraki, B.; Chilton, N. F.; Murray, K. S.; Schmitt, W.; Kruger, P. E. *Dalton Trans.* **2011**, *40*, 12368−12373.

(30) Weber, B.; Kaps, E. S.; Obel, J.; Achterhold, K.; Parak, F. G. *Inorg. Chem.* **2008**, *47*, 10779−10787.
(31) Amoore, J. L. M.; Kepert, C. J.; Cashion, J. D.; Moubaraki, B.; Neville, S. M.; Murray, K. S. *Chem.—Eur. J.* **2006**, *12*, 8220−8227.
(32) Gaspar, A. B.; Ksenofontov, V.; Reiman, S.; Gütlich, P.; Thompson, A. L.; Goeta, A. E.; Muñoz, M. C.; Real, J. A. *Chem.—Eur. J.* **2006**, *12*, 9289−9298.
(33) Ortega-Villar, N.; Thompson, A.; Muñoz, M. C.; Ugalde-Saldivar, V.; Goeta, A. E.; Moreno-Esparza, R.; Real, J. A. *Chem.—Eur. J.* **2005**, *11*, 5721−5734.
(34) Leita, B.; Moubaraki, B.; Murray, K.; Smith, J.; Cashion, J. *Chem. Commun.* **2004**, 156−157.
(35) Nakano, K.; Kawata, S.; Yoneda, K.; Fuyuhiro, A.; Yagi, T.; Nasu, S.; Morimoto, S.; Kaizaki, S. *Chem. Commun.* **2004**, 2892−2893.
(36) Nakano, K.; Suemura, N.; Kawata, S.; Fuyuhiro, A.; Yagi, T.; Nasu, S.; Morimoto, S.; Kaizaki, S. *Dalton Trans.* **2004**, 982−988.
(37) Gaspar, A.; Ksenofontov, V.; Martinez, V.; Munoz, M.; Real, J.; Gutlich, P. *Eur. J. Inorg. Chem.* **2004**, 4770−4773.
(38) Real, J. A.; Bolvin, H.; Bousseksou, A.; Dworkin, A.; Kahn, O.; Varret, F.; Zarembowitch, J. *J. Am. Chem. Soc.* **1992**, *114*, 4650−4658.
(39) Neville, S. M.; Moubaraki, B.; Murray, K. S.; Kepert, C. J. *Angew. Chem., Int. Ed.* **2007**, *46*, 2059−2062.
(40) Grunert, C. M.; Schweifer, J.; Weinberger, P.; Linert, W.; Mereiter, K.; Hilscher, G.; Müller, M.; Wiesinger, G.; van Koningsbruggen, P. J. *Inorg. Chem.* **2004**, *43*, 155−165.
(41) Halder, G. J.; Kepert, C. J.; Moubaraki, B.; Murray, K. S.; Cashion, J. D. *Science* **2002**, *298*, 1762−1765.
(42) Ohkoshi, S.; Imoto, K.; Tsunobuchi, Y.; Takano, S.; Tokoro, H. *Nature Chem.* **2011**, *3*, 564−569.
(43) Neville, S. M.; Leita, B. A.; Halder, G. J.; Kepert, C. J.; Moubaraki, B.; Létard, J.-F.; Murray, K. S. *Chem.—Eur. J.* **2008**, *14*, 10123−10133.
(44) Neville, S. M.; Halder, G. J.; Chapman, K. W.; Duriska, M. B.; Southon, P. D.; Cashion, J. D.; Létard, J.-F.; Moubaraki, B.; Murray, K. S.; Kepert, C. J. *J. Am. Chem. Soc.* **2008**, *130*, 2869−2876.
(45) Real, J. A.; Andrés, E.; Muñoz, M. C.; Julve, M.; Granier, T.; Bousseksou, A.; Varret, F. *Science* **1995**, *268*, 265−267.
(46) Halder, G. J.; Chapman, K. W.; Neville, S. M.; Moubaraki, B.; Murray, K. S.; Létard, J.-F.; Kepert, C. J. *J. Am. Chem. Soc.* **2008**, *130*, 17552−17562.
(47) Moliner, N.; Muñoz, C.; Létard, S.; Solans, X.; Menéndez, N.; Goujon, A.; Varret, F.; Real, J. A. *Inorg. Chem.* **2000**, *39*, 5390−5393.
(48) Adams, C. J.; Muñoz, M. C.; Waddington, R. E.; Real, J. A. *Inorg. Chem.* **2011**, *50*, 10633−10642.
(49) Morita, T.; Asada, Y.; Okuda, T.; Nakashima, S. *Bull. Chem. Soc. Jpn.* **2006**, *79*, 738−744.
(50) Neville, S. M.; Halder, G. J.; Chapman, K. W.; Duriska, M. B.; Moubaraki, B.; Murray, K. S.; Kepert, C. J. *J. Am. Chem. Soc.* **2009**, *131*, 12106−12108.
(51) Garcia, Y.; Niel, V.; Muñoz, M. C.; Real, J. A. *Top. Curr. Chem.* **2004**, *233*, 229−257.
(52) Adams, C. J.; Real, J. A.; Waddington, R. E. *CrystEngComm* **2010**, *12*, 3547−3553.
(53) Li, S. H.; Pang, S. P.; Li, X. T.; Yu, Y. Z.; Zhao, X. Q. *Chin. Chem. Lett.* **2007**, *18*, 1176−1178.
(54) Qi, C.; Li, S.-H.; Li, Y.-C.; Wang, Y.; Chen, X.-K.; Pang, S.-P. *J. Mater. Chem.* **2011**, *21*, 3221−3225.
(55) Nonius. *COLLECT*; Nonius BV: Delft, The Netherlands, 1998.
(56) Otwinowski, Z.; Minor, W. *Macromolecular Crystallography*, Part A; Methods in Enzymology, Vol. *276*; Carter, C. W., Jr., Sweet, R. M., Eds.; Academic Press: New York, 1997; pp 307−326.
(57) Blessing, R. H. *Acta Crystallogr.* **1995**, *A51*, 33−38.
(58) Blessing, R. *J. Appl. Crystallogr.* **1989**, *22*, 396−397.
(59) Sheldrick, G. M. *SHELXS97*, Program for Structure Solution; University of Göttingen: Göttingen, Germany, 1997.
(60) Sheldrick, G. M. *SHELXL97*, Program for Structure Refinement; University of Göttingen: Göttingen, Germany, 1997.
(61) Guionneau, P.; Marchivie, M.; Bravic, G.; Létard, J.-F.; Chasseau, D. *Top. Curr. Chem.* **2004**, *234*, 97−128.
(62) Boultif, A.; Louër, D. *J. Appl. Crystallogr.* **2004**, *37*, 724−731.
(63) Lee, J. J.; Sheu, H. S.; Lee, C. R.; Chen, J. M.; Lee, J. F.; Wang, C. C.; Huang, C. H.; Wang, Y. *J. Am. Chem. Soc.* **2000**, *122*, 5742−5747.
(64) Chernyshov, D.; Hostettler, M.; Törnroos, K. W.; Bürgi, H.-B. *Angew. Chem., Int. Ed.* **2003**, *42*, 3825−3830.
(65) Garcia, Y.; van Koningsbruggen, P. J.; Lapouyade, R.; Fournès, L.; Rabardel, L.; Kahn, O.; Ksenofontov, V.; Levchenko, G.; Gütlich, P. *Chem. Mater.* **1998**, *10*, 2426−2433.
(66) Giménez-López, M. C.; Clemente-León, M.; Coronado, E.; Romero, F. M.; Shova, S.; Tuchagues, J. P. *Eur. J. Inorg. Chem.* **2005**, 2783−2787.
(67) Yamada, M.; Hagiwara, H.; Torigoe, H.; Matsumoto, N.; Kojima, M.; Dahan, F.; Tuchagues, J. P.; Re, N.; Iijima, S. *Chem.—Eur. J.* **2006**, *12*, 4536−4549.
(68) Sugiyarto, K. H.; Craig, D. C.; Rae, A. D.; Goodwin, H. A. *Aust. J. Chem.* **1994**, *47*, 869−890.
(69) Marcén, S.; Lecren, L.; Capes, L.; Goodwin, H. A.; Létard, J.-F. *Chem. Phys. Lett.* **2002**, *358*, 87−95.
(70) Dîrtu, M. M.; Rotaru, A.; Gillard, D.; Linares, J.; Codjovi, E.; Tinant, B.; Garcia, Y. *Inorg. Chem.* **2009**, *48*, 7838−7852.
(71) Coronado, E.; Galán-Mascarós, J. R.; Monrabal-Capilla, M.; García-Martínez, J.; Pardo-Ibáñez, P. *Adv. Mater.* **2007**, *19*, 1359−1361.
(72) Prins, F.; Monrabal-Capilla, M.; Osorio, E. A.; Coronado, E.; van der Zant, H. S. J. *Adv. Mater.* **2011**, *23*, 1545−1549.
(73) Lin, Y.-C. Bond Characterization and Electronic Configuration of Ti, Mn and Fe Complexes. Ph.D. Thesis, Department of Chemistry, National Taiwan University, Taipei, Taiwan, 2006.
(74) Katz, B. A.; Strouse, C. E. *Inorg. Chem.* **1980**, *19*, 658−665.
(75) Sorai, M.; Ensling, J.; Hasselbach, K. M.; Gütlich, P. *Chem. Phys.* **1977**, *20*, 197−208.
(76) Grosjean, A.; Daro, N.; Kauffmann, B.; Kaiba, A.; Létard, J.-F.; Guionneau, P. *Chem. Commun.* **2011**, *47*, 12382−12384.